Supporting Information

Formation of Electron-deficient Ni in Nb/NiFe-Layered Double Hydroxide Nanoarray by Electrochemical Activation for Efficient Water Oxidation

Metohds

1.1 Materials:

Various chemicals were used in this study. $Fe(NO3)_2·9H_2O$ (99.99%), $NbCl_5$ (99.9%)and Nickel(II) Acetyl Acetonate ($Ni(acac)_2$, 99%) were purchased from Aladdin Industrial Co. Urea (99%) and ethanol (99.9%) were purchased from Beijing Chemical Reagents Co. Carbon fiber paper was purchased from Toray Industries, Inc. Deionized water with a resistivity ≥ 18 MΩ was used to prepare all aqueous solutions. All the reagents were of analytical grade and were used directly without further purification.

1.2 Synthesis of NiFe-LDH:

Firstly, 1 mmol $Ni(acac)_2$, 1 mmol $Fe(NO3)_2·9H_2O$, and 0.3 g urea were dissolved in 30 mL deionized water. Then this solution and a piece of 2*4 cm cleaned Ni foam was transferred into the Teflon-lined stainless autoclave and maintained at 120°C for 12 h to obtain the NiFe-LDH.

1.3 Synthesis of Nb/NiFe-LDH:

Firstly, 1 mmol $Ni(acac)_2$, 1 mmol $Fe(NO3)_2·9H_2O$, 0.15 mmol NbCl5 and 0.3 g urea were dissolved in 30 mL deionized water. Then this solution and a piece of 2*4 cm cleaned Ni foam was transferred into the Teflon-lined stainless autoclave and maintained at 120°C for 12 h to obtain the Nb/NiFe-LDH .

1.4 Physical characterization

SEM images were obtained on a Zeiss SUPRA55 scanning electron microscope, which was operated at 10 kV and the corresponding EDS elemental mappings were characterized using an energy dispersive spectrometer (Oxford).. HRTEM images were carried out by the JEOL JEM-2100 operating at 200 kV. XRD patterns were recorded on an Ultima IV (Rigaku) in the range from 10° to 70° at a scan rate of $5°/min^{-1}$. XPS were performed by using a model of K-Alpha (Thermo Scientific).

Raman spectra were recorded on a Lab RAM Aramis (HORIBA Jobin Yvon S.A.S, Laser 532). ICP-OES and ICP-MS were carried out by the Thermo Fisher iCAP 7400.

1.5 Electrochemical measurements

The electrochemical measurements for OER were performed in a standard three-electrode system at room temperature (25 °C) on an electrochemical workstation (CHI 660D, Chenhua, Shanghai), where Nb/NiFe-LDH,NiFe -LDH and Ni foam serve as the working electrodes, while Pt foil electrode and SCE electrode serve as counter electrode and reference electrode, 1 M KOH were used as the electrolyte, respectively. The LSV tests at a scan rate of 5 mV s^{-1} were performed after 40 cycles of CV. The final potentials were converted with respect to the reversible hydrogen electrode (RHE) based Nernst equation:

$$\mathrm{E\,(RHE,\ iR\ corrected)} = \mathrm{E(SCE)} + 0.244\ \mathrm{V} + 0.059\ \mathrm{pH} - \mathrm{iR} \quad (1)$$

where i is the measured current density and R is the solution resistance determined by electrochemical impedance spectroscopy at a high frequency. The Tafel plots were derived from polarization curves at low overpotentials fitted to the Tafel equation:

$$\eta = a + b \log J \quad (2)$$

where η is the overpotential, J is the current density, a and b are constants. The CP tests were carried out at current densities of 0.01 and 0.1 A cm^{-2} in a two-electrode system using 1 M KOH electrolyte with a piece of Ni foam as a cathode and Nb/NiFe-LDH as an anode. The obtained data for CP tests for stability were not iR corrected and displayed as raw data.

Then ECSA can be determined by dividing Cdl by the specific capacitance, as shown in Equation :

$$\mathrm{ECSA} = \frac{C_{dl}}{C_s} \quad (3)$$

where Cs is 0.04 mF cm^{-2} based on values reported for metal electrodes in an aqueous alkaline solution. Cdl was obtained from CV in a non-Faraday region with scan rates of 10, 20, 30, 40, 50, 60, 70, 80, 90 and 100 mV s^{-1}.

1.6 AEM electrolyzer fabrication

The AEM electrolyzer was assembled with an anode (4.0 cm^2), cathode(4.0 cm^2), and anion exchange membrane (AEM, Versoge A20). Nb/NiFe-LDH as the anode and Ni foam as the cathode to construct the Nb/NiFe-LDH ||Ni foam AEM electrolyzer. The assembly of the AEM electrolyzer required no additional process, such as heating or pressing. We studied the performance of the AEM electrolyzer in a 1.0 M KOH electrolyte at 80 ± 2 °C, using a potentiostat. The polarization curve was measured using LSV technology at a scan rate of 5 mV s^{-1}. The durability test was carried out by CP technology at a current density of 1.0 A cm^{-2} for over 100 h at 80 ± 2 °C, 1 M KOH were used as the electrolyte.

1.7 Operando electrochemical Raman measurements

Electrochemical Raman spectroscopy was carried out on a Horiba Lab RAM HR Evolution confocal Raman spectrometer with a 532 nm laser source, a 50× objective and an acquisition time of 90 s. And the electrochemical workstation (CHI 660D, Chenhua, Shanghai) were used to performed the Amperometric i-t Test under OCP-1.37 V vs RHE, respectively.

1.8. DFT calculations

Density functional theory (DFT) calculations were performed using the projector wave method in the Vienna Ab initio Simulation Package (VASP) [1, 2]. The Perdew-Burke-Ernzerhof (PBE) generalized gradient approximation (GGA) was used to calculate the exchange and associated energy density functions [3, 4]. The lattice parameters of the caculation model have been optimized to a, b, c, α, β, and γ values of 8.95 Å, 10.83 Å, 21.26 Å, 90◦, 90◦, and 90◦, respectively. For the thermodynamic calculations, the three lower layers were held in place, while the upper layers were released. The bulk and slab models were optimized using the Gamma type K-point sampling parameters of 5×5×5 and 3×3×1 respectively. 0.02 *e*V/Å a and 10^{-5} *e*V were used as convergence criteria for the force and the energy, the cut-off energy

was 500 eV. We have used a vacuum region of 15 Å between the surfaces which we confirmed is sufficient to eliminate the surface–surface artefact interaction.

The free energy of the electrochemical reaction was determined using the Computational Hydrogen Electrode Method by relating the chemical potential of the proton-electron pair at the reversible hydrogen electrode (RHE) potential to half the Gibbs free energy per molecule of hydrogen. Furthermore, Δ*ZPE*, Δ*S*, denote the change of zero point energy obtained from the DFT calculation and the change of entropy obtained from the calculation of the vibration frequency y at T = 298.15K, respectively [5]. We have also calculated more accurate energies (*E*), zero point energies (*ZPE*) and entropies (*S*) for H_2, H_2O and O_2 as shown in Table S1. Moreover, U was the electrode potential relative to the reversible hydrogen electrode (RHE). The catalytic activity of a material could be well measured by expressing the offset of the electrode potential from the standard electrode potential through the overpotential (η)[6], which is expressed in equation (1).

$$\eta = \max\frac{[\Delta G(1),\Delta G(2),\Delta G(3),\Delta G(4)]}{e} - 1.23\text{V} \quad (1)$$

Table S1. Energy, *ZPE*, and entropy (*e*V) for molecules.

	E	*ZPE*	*TS*
H_2(g)	-6.76	0.347	0.40
O_2(g)	-8.81	0.134	0.63
H_2O(l)	-14.22	0.570	0.67

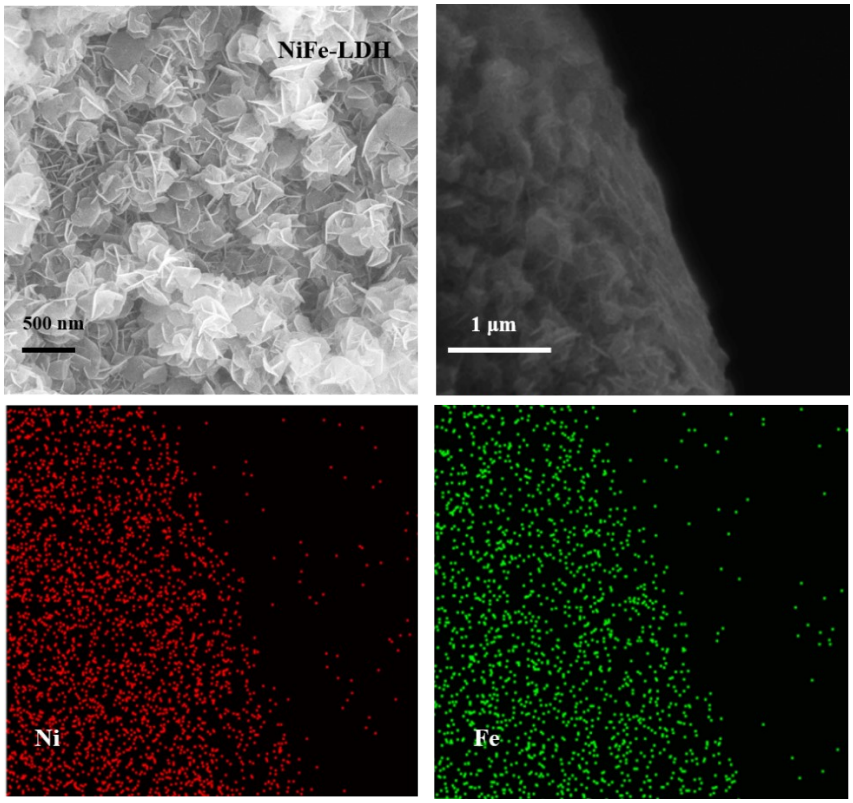

Supplementary Figure 1| Schematic of preparing process and SEM image of NiFe-LDH.

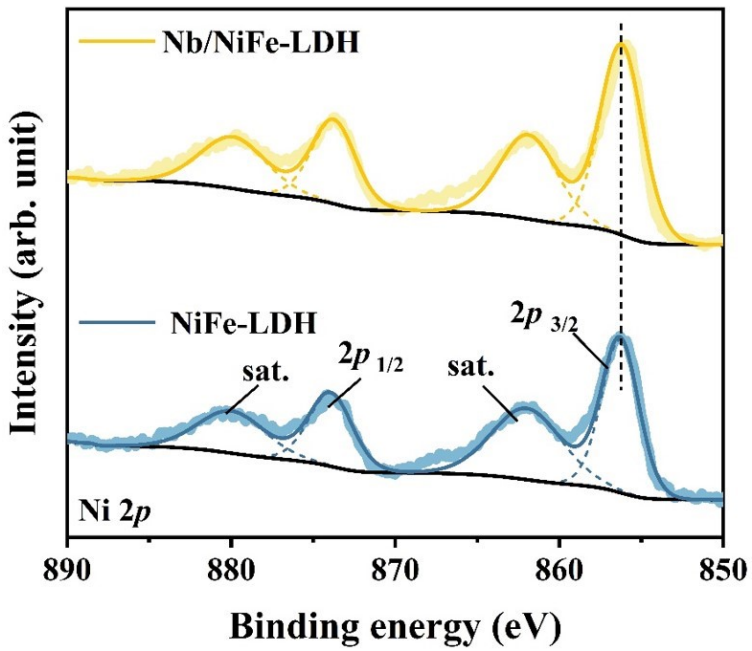

Supplementary Figure 2| XPS spectra of Ni 2p for Nb/NiFe-LDH and NiFe-LDH before activation.

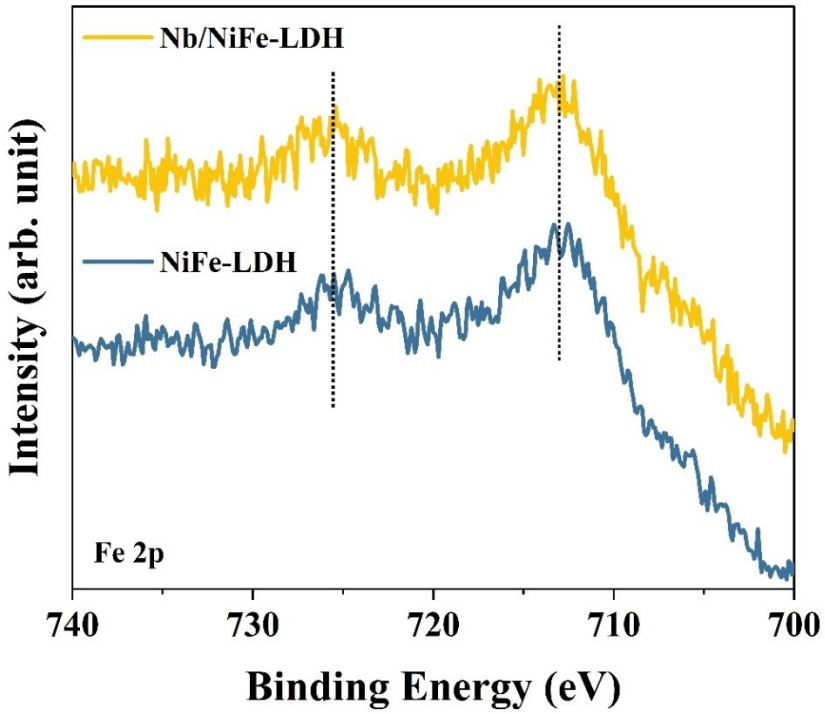

Supplementary Figure 3| XPS spectra of Fe 2p for Nb/NiFe-LDH and NiFe-LDH before activation.

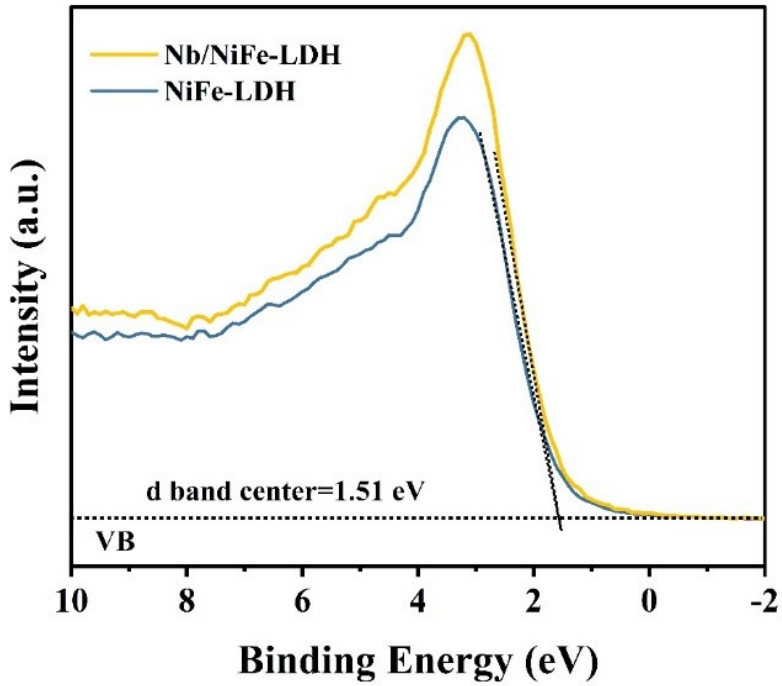

Supplementary Figure 4| XPS valence band spectra of Nb/NiFe-LDH and NiFe-LDH.

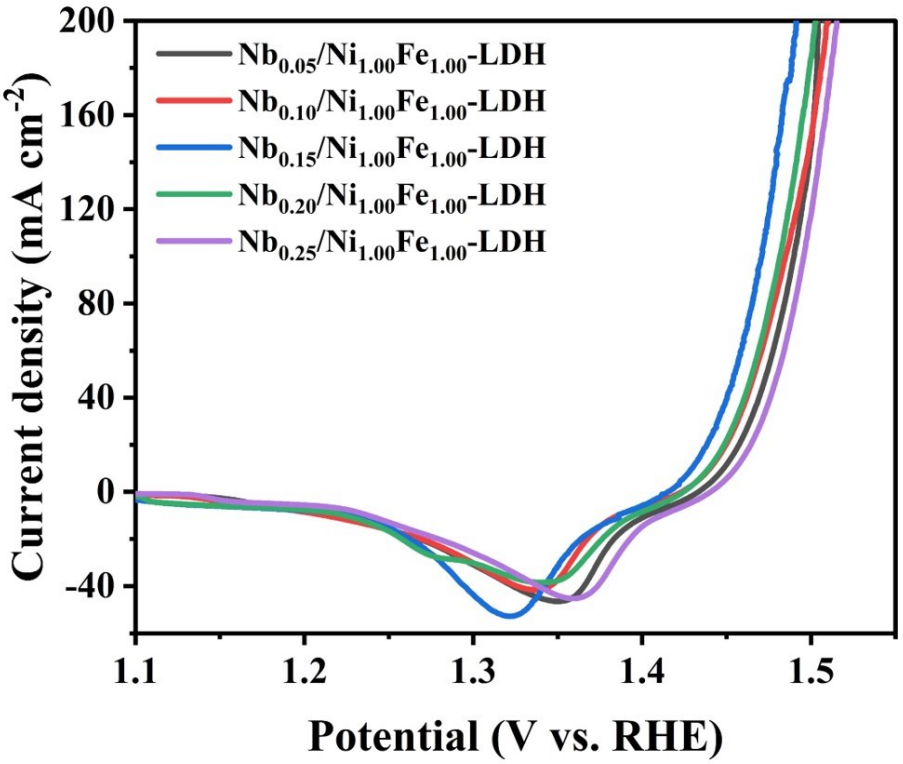

Supplementary Figure 5| The LSV curves of Nb/NiFe LDH with different metal ratio.

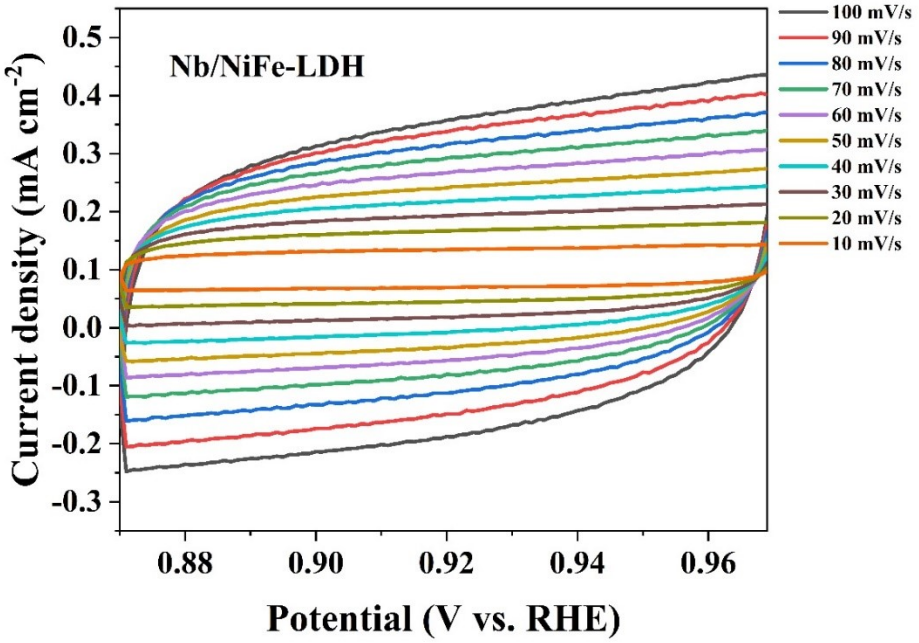

Supplementary Figure 6| CV curves of Nb/NiFe-LDH in 1 M KOH at the scan rate of 10, 20, 30, 40, 50, 60, 70, 80 , 90, 100 mV s^{-1}.

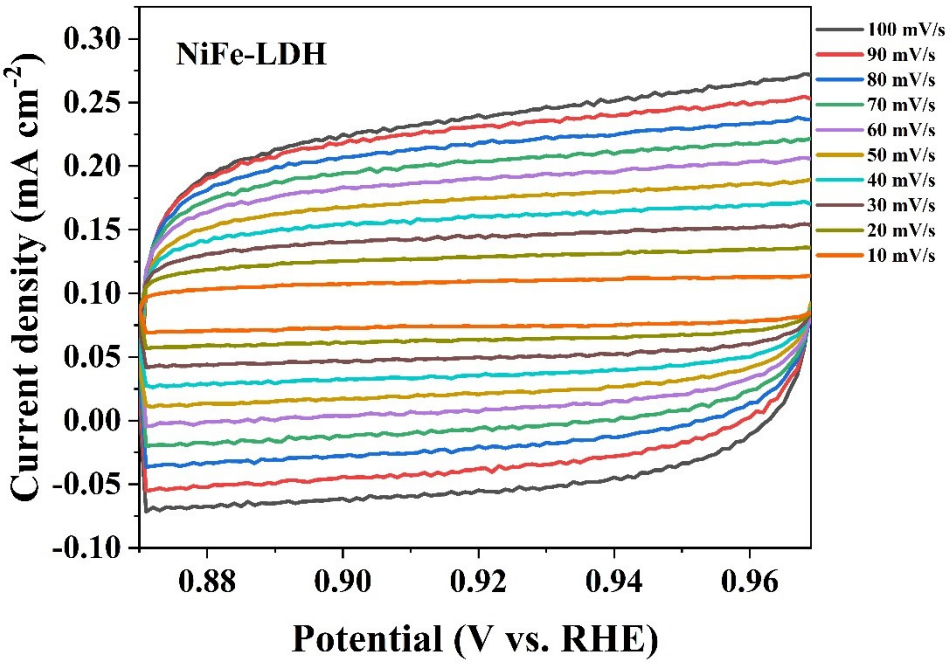

Supplementary Figure 7| CV curves of NiFe-LDH in 1 M KOH at the scan rate of 10, 20, 30, 40, 50, 60, 70, 80 , 90, 100 mV s^{-1}.

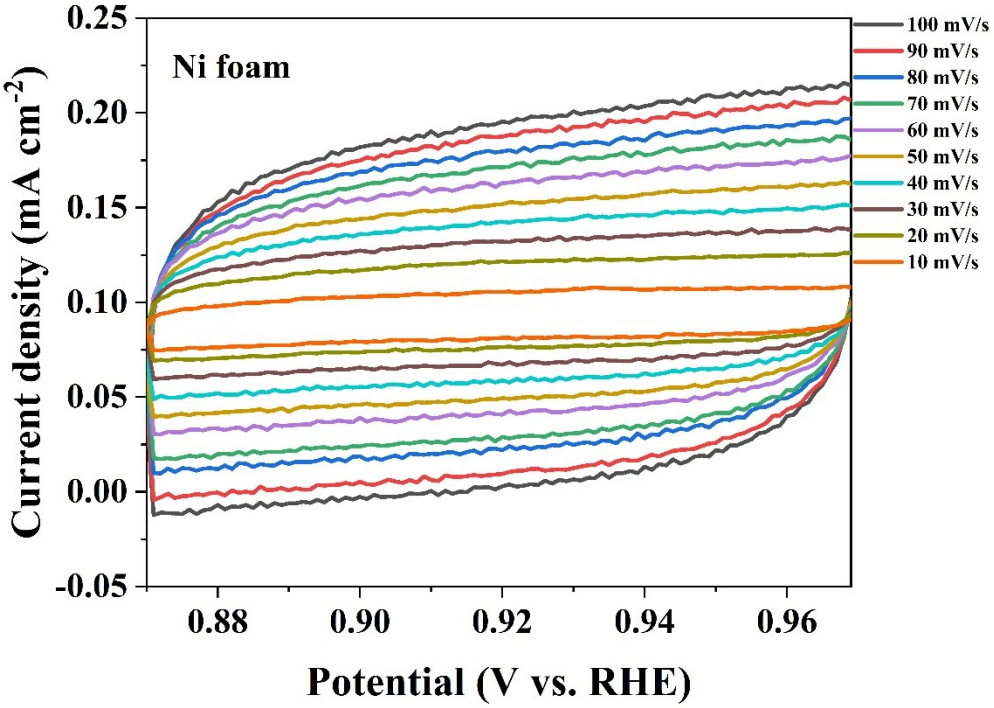

Supplementary Figure 8| CV curves of Ni foam in 1 M KOH at the scan rate of 10, 20, 30, 40, 50, 60, 70, 80 , 90, 100 mV s^{-1}.

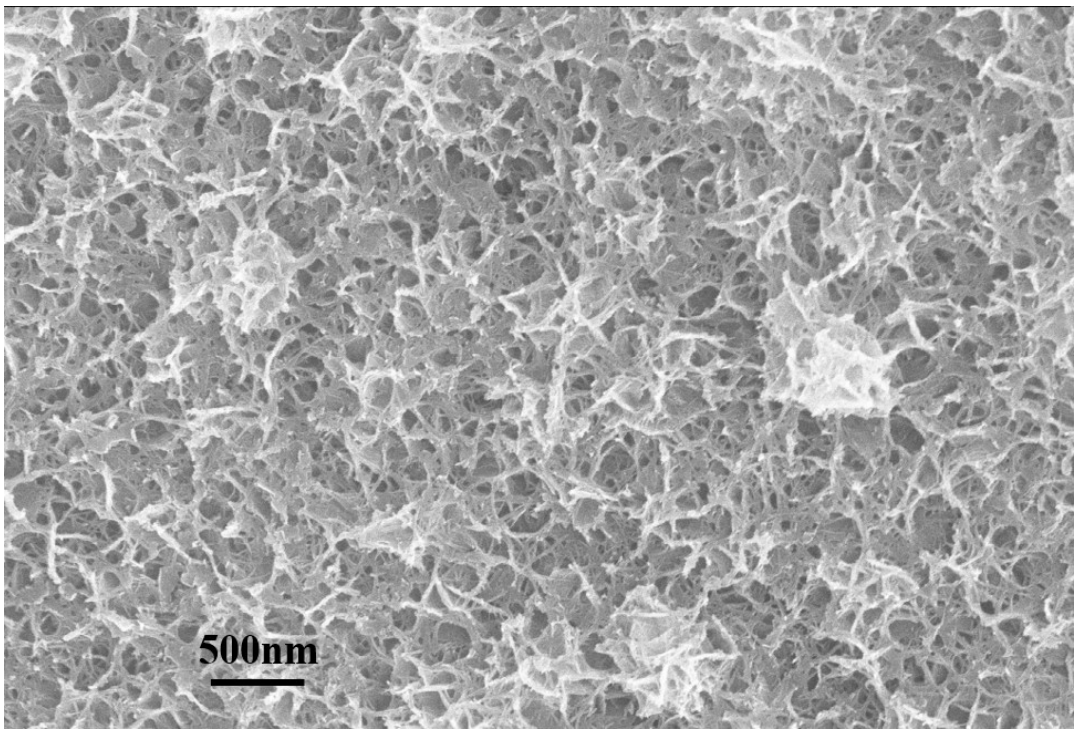

Supplementary Figure 9| SEM image of NiFe-LDH after activation.

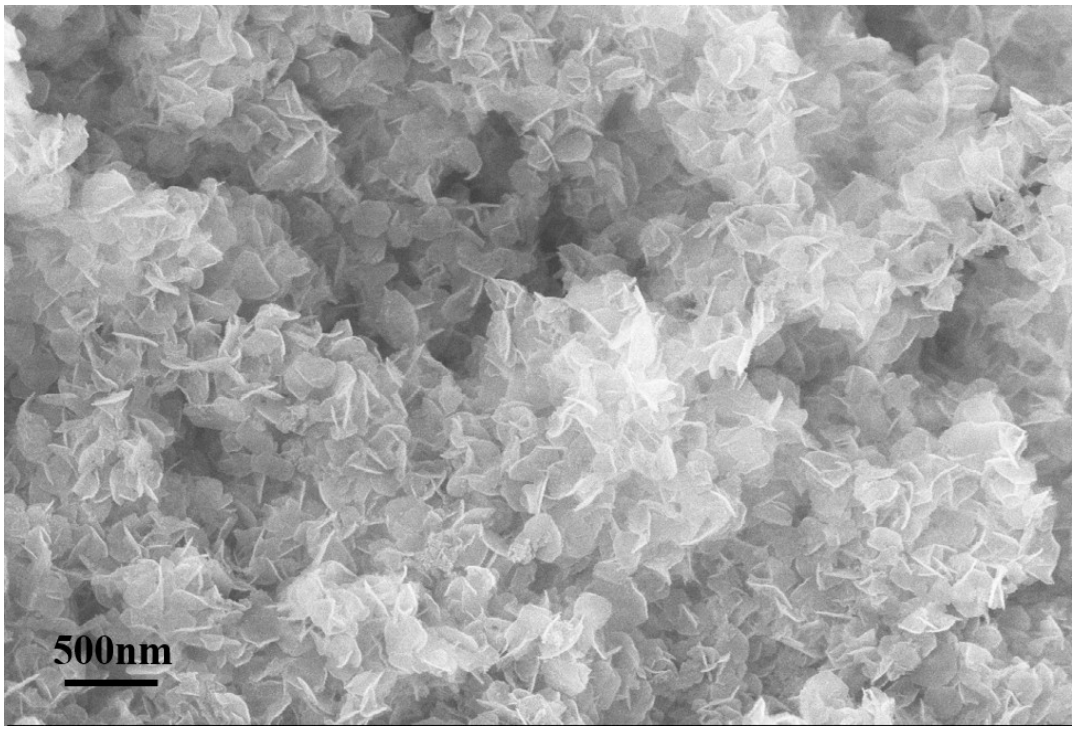

Supplementary Figure 10| SEM image of Nb/NiFe-LDH after activation.

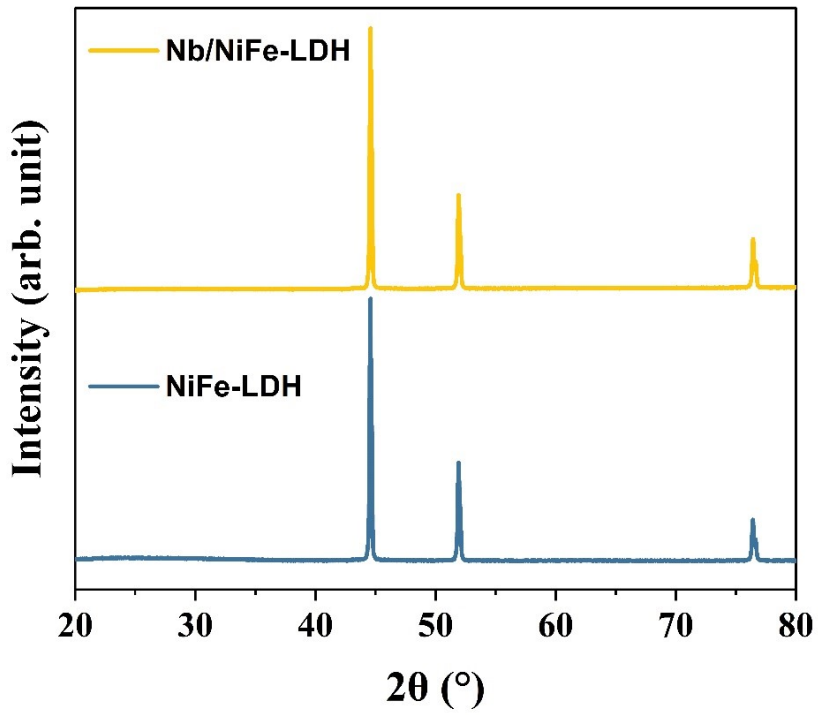

Supplementary Figure 11| The XRD patterns of Nb/NiFe-LDH and NiFe-LDH after activation.

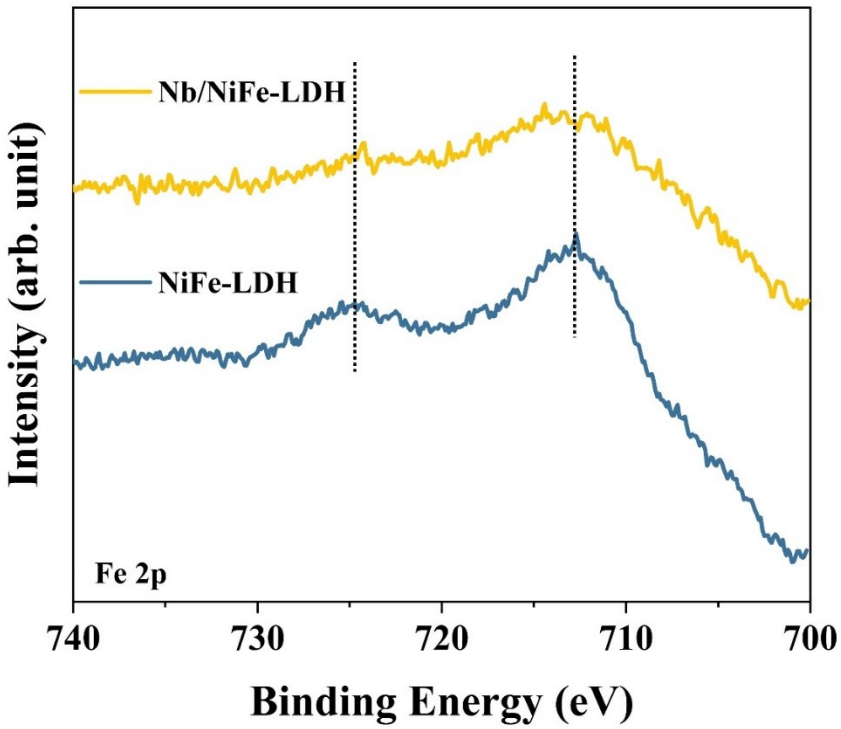

Supplementary Figure 12| Schematic of preparing process and SEM image of NiFe-LDH; XPS spectra of Fe 2p for Nb/NiFe-LDH and NiFe-LDH after activation.

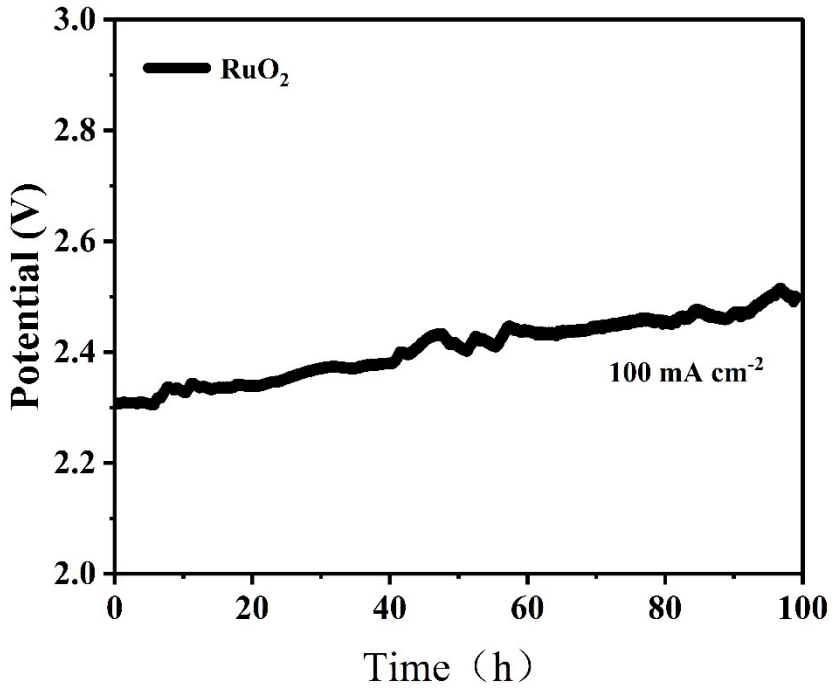

Supplementary Figure 13| Stability test of RuO_2 at current density of 0.01 A/cm^2.

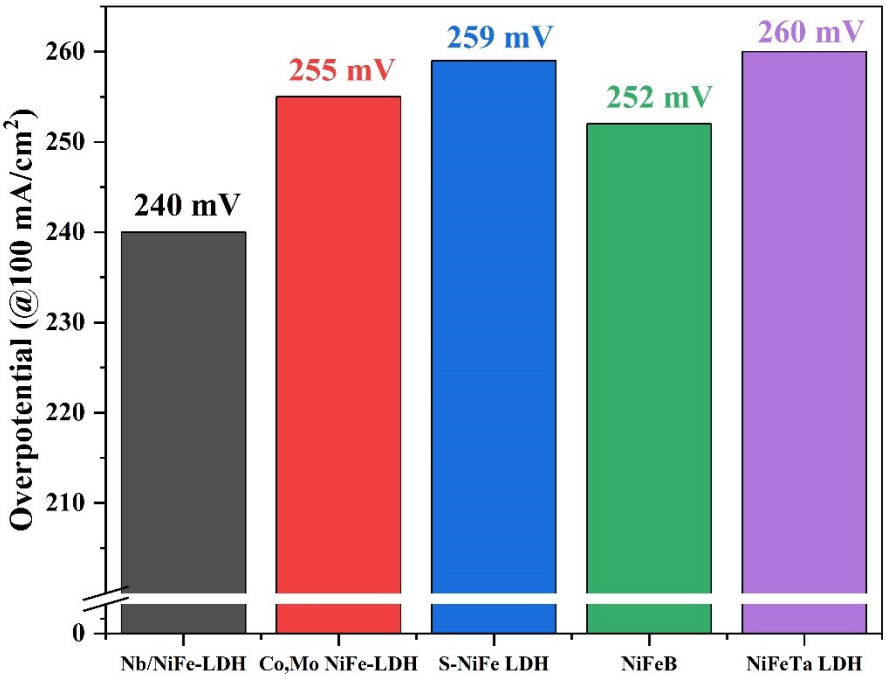

Supplementary Figure 14| Comparison of alkaline OER activity between Nb/NiFe-LDH and differently doped NiFe-LDH.[7-10]

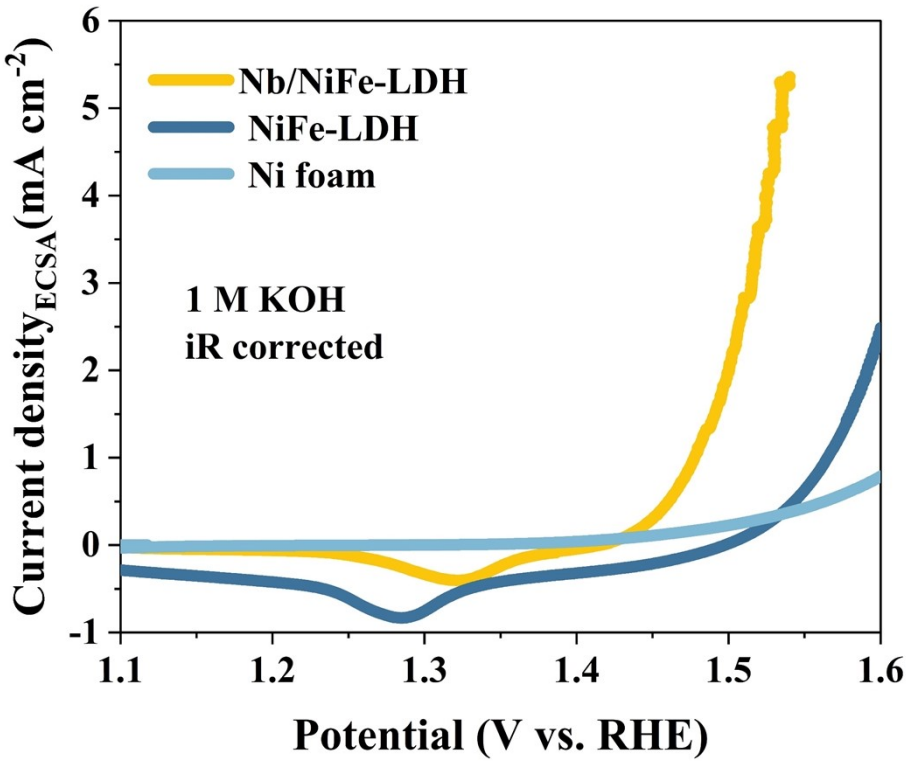

Supplementary Figure 15| Linear sweep voltammetry curves normalized by ECSA.

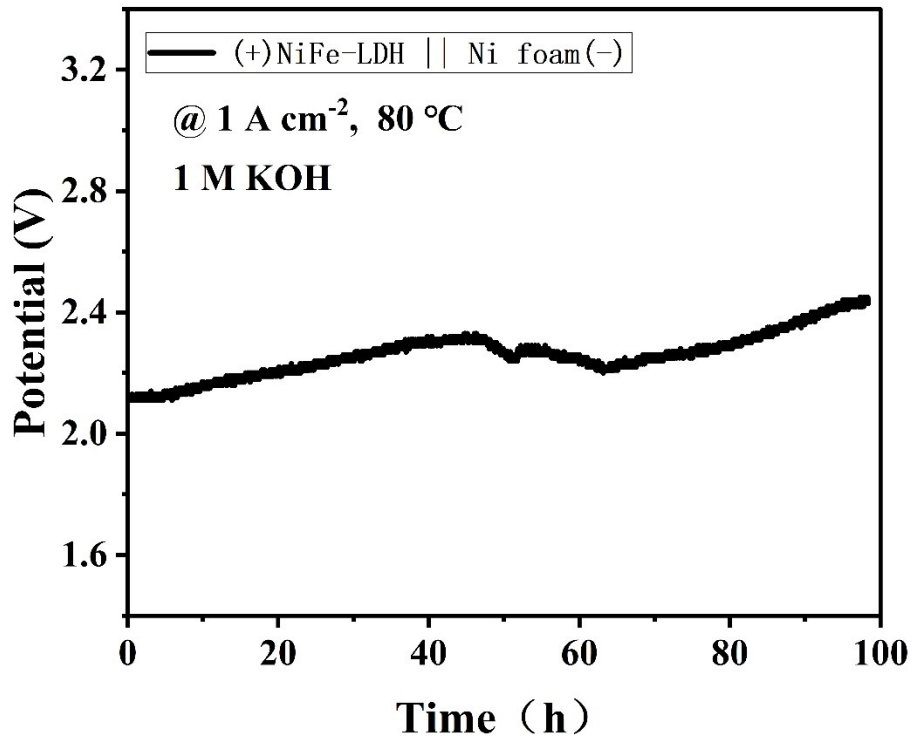

Supplementary Figure 16| Durability test of the AEM electrolyzer using NiFe-LDH || Ni foam at 1.0 A/cm^2 in 1.0 M KOH.

Reference

1. G. Kresse and J. Furthmüller, *Computational Materials Science*, 1996, **6**, 15-50.
2. G. Kresse and J. Furthmüller, *Physical Review B*, 1996, **54**, 11169-11186.
3. P. E. Blöchl, *Physical Review B*, 1994, **50**, 17953-17979.
4. G. Kresse and D. Joubert, *Physical Review B*, 1999, **59**, 1758-1775.
5. M. Bajdich, M. García-Mota, A. Vojvodic, J. K. Nørskov and A. T. Bell, *Journal of the American Chemical Society*, 2013, **135**, 13521-13530.
6. J. Rossmeisl, A. Logadottir and J. K. Nørskov, *Chemical Physics*, 2005, **319**, 178-184.
7. Y. Zhao, Q. Wen, D. Huang, C. Jiao, Y. Liu, Y. Liu, J. Fang, M. Sun and L. Yu, *Advanced Energy Materials*, 2023, **13**.
8. X. Wang, Y. Tuo, Y. Zhou, D. Wang, S. Wang and J. Zhang, *Chemical Engineering Journal*, 2021, **403**.
9. H. Lei, L. Ma, Q. Wan, S. Tan, B. Yang, Z. Wang, W. Mai and H. J. Fan, *Advanced Energy Materials*, 2022, **12**.
10. Y. Bai, Y. Wu, X. Zhou, Y. Ye, K. Nie, J. Wang, M. Xie, Z. Zhang, Z. Liu, T. Cheng and C. Gao, *Nature Communications*, 2022, **13**.